Experimental investigation of surface wettability induced anti-icing characteristics in an ice wind tunnel

Haoyang Sun[a], Guiping Lin[a], Haichuan Jin[a,*], Xueqin Bu[a], Chujiang Cai[b], Qi Jia[c],

Kuiyuan Ma[a], Dongsheng Wen[a,d]

[a] *Laboratory of Fundamental Science on Ergonomics and Environmental Control, School of Aeronautic Science and Engineering, Beihang University, Beijing 100191, China*

[b] *Ministry-of-Education Key Laboratory of Fluid Mechanics, School of Aeronautic Science and Engineering, Beihang University, Beijing 100191, China*

[c] *AECC Shenyang Engine Research Institute, Shenyang 110015, China*

[d] *School of Chemical and Process Engineering, University of Leeds, Leeds, LS2 9JT, UK*

Abstract: Turbine blade icing is a serious threat for the safety of wind power generation. Low energy ice protection techniques especially those using superhydrophobic surfaces, have attracted intensive interest recently. In this work, the anti-icing characteristics of wind turbine blade have been investigated in an ice wind tunnel, and the influence of the surface wettabilities, preparation methods on the ice protection performance and the durability of different surface materials have been examined experimentally. It is found that the surface wettability can dramatically change the ice protection characteristics. Superhydrophobic surfaces prepared by both spraying and laser ablation methods can efficiently reduce the energy consumption of the electrothermal system, and the maximum conserved energy reaches 76.7% when the temperature of heating surface is lower than 15°C. The surface tension induced flow pattern change of runback water should be responsible for the energy efficient anti-icing, i.e., the runback water sheds from the superhydrophobic surface rapidly, preventing the runback icing on the surface. Droplets impacting can damage the wettabilities and the superhydrophobic surface prepared by laser ablation method has the best durability during the ice wind tunnel test. The concept of superhydrophobic-dry anti-icing has been proposed in this paper, which is very promising in solving the icing issue of wind turbine blade with low energy consumption.

Key words: Superhydrophobic surface, Wind turbine blade icing, Anti-icing, Ice protection, Ice wind tunnel, Durability

[*] Corresponding author, Email: jinhaichuan@buaa.edu.cn

1. Introduction

Wind energy is the most promising clean and renewable energy, which has a wide range of application prospects[1]. According to the Global Wind Energy Report[2] issued by the Global Wind Energy Council, the global wind power generation is about 1340 TWh, accounting for about 5% of the world's total power generation in 2019. The global new installed capacity is 93GW, bringing the global cumulative wind power capacity to 743 GW in 2020. With the rapid development of wind power generation, the utilization of wind energy in cold climates has received more and more attention. In cold climates, wind power generation efficiency benefits from the higher wind speed and air density[3, 4]. However, low air temperature causes the wind turbine blade to face icing problem, challenging the normal operation of wind turbine. On the one hand, ice accumulation changes the aerodynamic shape of the blade and reduces the power generation efficiency dramatically. On the other hand, ice accumulation causes the vibration of the blade, increasing the fatigue load and the maintenance cost of the blade. In addition, irregular ice shedding from the blade poses a great threat to the safety of human and the surrounding facilities[5-7]. Therefore, it is very urgent to solve the icing issue of wind turbine blade and develop reliable ice protection techniques.

The problem of wind turbine blade icing is very complicated, especially when coupled with flow field conditions, temperature, LWC (Liquid Water Content), and MVD (Median Volume Diameter)[8]. At low air temperature and LWC, the supercooled water droplets freeze and form rime ice immediately when impacting the blade surface. When the air temperature is near 0℃ and the LWC is high, only a small amount of supercooled water droplets freeze in the impact zone, and the others flow downstream then form glaze ice in the runback zone[5]. Aiming to investigate the icing problem of wind turbine blade, some researchers use simulative methods[9-19]. The icing calculation needs to accurately describe the form of liquid water, which is normally computationally consuming. For the simulation of blade icing, researchers have proposed Messinger model[20], Myers model[21, 22], Shallow Water Icing model (SWIM)[23], FFICE model[6], etc.. However, the above models simplify the runback water to a continuous water film, which cannot effectively predict the ice formation when surface wettability is under consideration. Ice wind tunnel has been employed to investigate the icing production of wind turbine blade[8, 15, 24-28], and many researches concentrates on the factors such as the blade airfoil, AoA (Angle of Attack), air speed, air temperature, MVD and LWC.

The simulation and experimental studies on the wind turbine blade icing point out the direction for the anti-/de-icing method[12, 29]. At the present, many anti-/de-icing systems have been applied to wind turbine blade, which are initially proposed for ice protection of the aircraft. Traditional anti-/de-icing methods can be divided into two categories, namely passive method and active method[30]. The passive method usually refers to the use of the physical characteristics of the blade surface, such as hydrophobic surfaces[31-33] and sunlight-responsive amphiphilic surface[34], to delay or prevent the blade from icing. The active method requires the input of external energy for anti-/de-icing, mainly including thermal anti-/de-icing methods (e.g., hot air injection, electric heating, etc.), mechanical deicing methods (e.g., expansion tubes, electric pulses, etc.), and liquid anti-icing methods (e.g., spraying low-freezing point anti-icing liquids, liquid supply from microporous metal, etc.). Among the above methods, thermal anti-/de-icing methods are considered to be the most effective for icing protection[35], among which hot air injection and electrothermal anti-/de-icing methods are the most commonly used[8]. However, hot air injection anti-/de-icing method requires the application of complex air pipelines, causing large amount of heat loss during the anti-/de-icing process, which consumes high energy for anti-/de-icing. Although electrothermal anti-icing method[36-39] has lower energy consumption in comparison to the hot air injection anti-/de-icing method, the power required by the heating component could reach up to 15% of the output power of the wind turbine[8], which significantly reduces the power generation efficiency.

In recent years, the research on ice protection techniques with low energy consumption attracts more and more attention, especially hydrophobic surface related[40-43]. Since Kao et al.[44, 45] successfully prepared artificial superhydrophobic surface for the first time in the mid-1990s, superhydrophobic surfaces have developed rapidly[46], with some potentially employed in anti-/de-icing process[47-52]. Normally, the unique wettability of superhydrophobic surfaces (i.e., contact angle greater than 150°, sliding angle less than 5°) exhibits icephobic performance, which plays a key role in supercooled water droplets impact, liquid water runback, and ice adhesion. Researches[53-56] showed that superhydrophobic surfaces could cause the supercooled droplets to break up and rebound during the impact, and reduce the contact time with the surface, hence preventing freezing. As described in a recent study by Antonini et al.[56], the contact time between droplet and surface was shortened with the increase of contact angle at the condition of droplet diameter of 2.4~2.6mm, impact velocity of 0.8~4.1 m/s and Weber number of 25~585. For the water runback, studies find that the superhydrophobic surfaces reduce the flow resistance between the liquid water and the surface, which causes the liquid water flow downstream quickly along the surface, resulting in lower thickness of the water film and prompting the water film to break into a rivulet or even a bead flow[57-59]. In addition, the superhydrophobic surfaces make the liquid water appear in the Cassie-Baxter state on its surface, and the air in the surface voids reduces the convective heat transfer coefficient, thereby delaying the time for water to freeze[60-62]. Regarding the icing adhesion, studies consider that superhydrophobic surfaces greatly reduce static icing adhesion[57, 63-65], which is closely related to surface roughness[66]. However, the icing adhesion increases when the droplet impacts on superhydrophobic surface with high speed[67], which is mainly due to the invasion of the supercooled water droplets into the surface microstructure.

Although experiments show that the superhydrophobic surfaces have potential in the anti-/de-icing process, they are still facing the drawbacks in ice protection of wind turbine blade. Recently, studies[31, 57] show that superhydrophobic surface can reduce the icing mass and the icing area in ice wind tunnel experiment, but it cannot completely prevent ice formation on the surface. The reason is that when impacting the unheated superhydrophobic surface, supercooled water droplets freeze immediately on the leading edge, which causes the failure of the icephobic properties. In order to avoid icing on the leading edge of the superhydrophobic surface, the electrothermal anti-icing system combined with superhydrophobic surface was designed[58, 59, 68, 69]. Pauw et al.[68] investigated the influence of superhydrophobic area on the ice protection performance of an electrothermal system, and concluded that the superhydrophobic surface played an important role in the 5%-10% chord length from the leading edge of the airfoil. Hu et al.[35] investigated the required anti-icing power of different heating areas, and found that covering only 5%—10% chord length of the blade front surface had the optimal anti-/de-icing performance when all of the surface was superhydrophobic. It is expected that the capability of ice protection should be closely related to the preparation methods and the wettability of the surface. However, it is noticed that in all of the above studies, the superhydrophobic surfaces were prepared by a specific preparation method. The comparison of surfaces with different wettabilities (i.e., hydrophilic, hydrophobic and superhydrophobic) and superhydrophobic surfaces prepared by different methods is still unclear. What’s more, few researchers investigate the durability of superhydrophobic surfaces, which should be closely related to the application in ice protection of wind turbine blade.

Aiming at addressing such limitations, an experimental work in this study was conducted on the surface wettability induced ice protection characteristics in an ice wind tunnel. An electrothermal anti-/de-icing system combined with different surfaces were examined for the comparison of energy consumption. The ice protection performance of hydrophilic, hydrophobic and superhydrophobic surfaces were carefully compared during the experiment. The superhydrophobic surfaces prepared by spraying method and laser ablation method were compared under the same icing condition. The contact angle and sliding angle were investigated before and after the ice wind tunnel experiments, aiming to evaluate the durability of different surfaces.

2. Experiment setup

2.1 Preparation of surfaces

For the current investigation, two kinds of superhydrophobic surface from different preparation methods , one kind of hydrophobic surface and one kind of hydrophilic surface were prepared before the experiment. The substrate for preparation of superhydrophobic and the hydrophobic surface was aluminum alloy with an average size of 0.15mm thickness, and the hydrophilic surface is the aluminum alloy itself. The superhydrophobic surfaces were prepared by spraying method and laser ablation method, respectively. The spraying method is mainly divided into three steps: pretreating substrate surface, painting surface with resin adhesive layer and spray-coating superhydrophobic nanomaterial, and details can be seen in our previous work[70]. For the current painting and spray-coating process, a 10 wt% acrylic resin solution and a 2 wt% fluorinated SiO_2 nanoparticle solution were employed. The roughness of the superhydrophobic surface was measured with SuperView W1 optical 3D surface profiler. As shown in **Fig. 1**(**a**), the surface roughness of the superhydrophobic surface is about 15μm, indicating a micro-level structure. In addition, the fluorinated SiO_2 nanoparticles form nano-level structure on the coatings.

Another kind of superhydrophobic surface and hydrophobic surface were prepared by laser ablation method, which was mainly divided into three steps: pre-treatment of the substrate surface, laser ablation and post-treatment of chemical modification. In the step of pretreating substrate surface, acetone was used to ultrasonically clean the substrate surface for 5-10 minutes. Then the surface was dried by compressed air for a period of time to ensure that there were no residual water or other impurities on the surface. In the step of laser ablation, a femtosecond laser (TRUMPF, TruMicro 5000) has been applied to fabricate well-designed structures combining microgrooves on the substrate surface. The superhydrophobic surface prepared by laser ablation method was with microgroove depth of 10-15μm and microgroove width of 5μm. What's more, the ablation interval of superhydrophobic surfaces was 50μm. In the step of posttreatment, the laser ablated surface and a glass slide dripped with fluorosilane (preparing for superhydrophobic surface) or Gentoo™ coating (Ultratech Company, preparing for hydrophobic surface) was placed inside a vacuum tube furnace. The temperature of the vacuum tube furnace was maintained around 60℃ for 2-4 hours for the chemical modification of the surface. The morphology of the resulting surface after laser ablation was observed by SEM (ZEISS, SIGMA 500). As shown in **Fig. 1**(**b**), the surface after lase ablation has micro to nano-level structure.

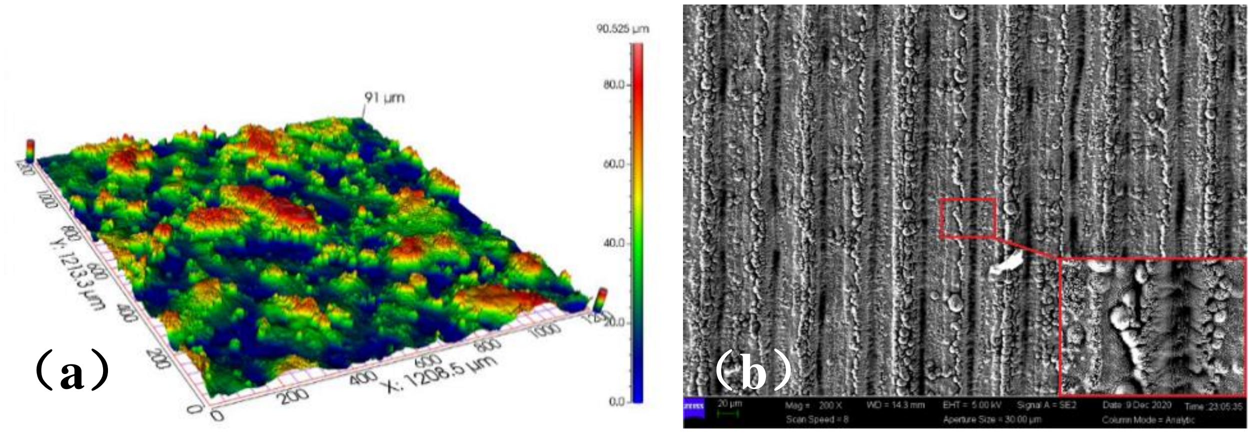

Fig. 1. (**a**) The surface roughness of superhydrophobic surface prepared by spraying method; (**b**) SEM image of surface prepared by laser ablation method.

For the convenience of description, in this paper the superhydrophobic surface prepared by spraying method is named SP-FNS (Spray method-Fluorinated Nanosilica), the superhydrophobic surface modified with fluorosilane prepared by laser ablation method is named LA-FS (Laser Ablation method- fluorosilane), the hydrophobic surface modified with Gentoo^{TM} surface prepared by laser ablation method is named LA-GT (Laser Ablation method-Gentoo^{TM}), and the surface of aluminum alloy is named ALA (Aluminium Alloy). The wettabilities of the above surfaces were tested by using a similar procedure as described in Waldman et al.[71] and Korhonen et al.[72], as shown in **Fig. 2** and **Table 1**.

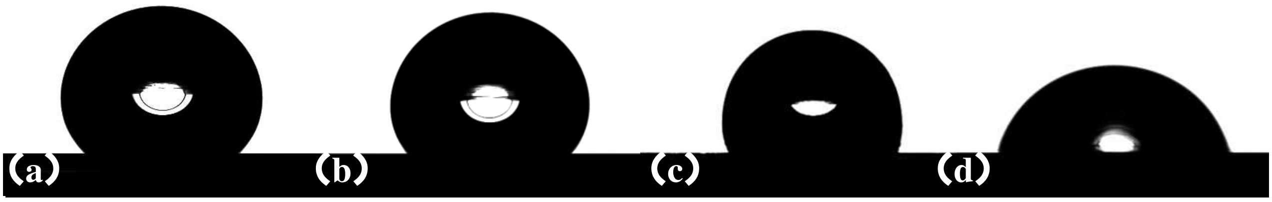

Fig. 2. Contact angle of (**a**) SP-FNS; (**b**) LA-FS; (**c**) LA-GT; (**d**) ALA

Table 1. Contact angle and sliding angle of different surfaces

Surfaces	SP- FNS	LA-FS	LA-GT	ALA
Contact Angle (°)	153.4±2	156.0±2	112.7±2	77.8±2
Sliding Angle (°)	4.5±2	3.0±2	16.8±2	28.3±5
Advancing angle (°)	155.9±2	158.2±2	124.8±2	98.1 ±2
Receding angle (°)	150.7±2	152.5±2	103.6±2	62.4±2
Hysteresis (°)	5.2±4	5.7±4	21.2±4	35.7±4

2.2 Test section design

All of the following experiments were conducted in the reflux ice wind tunnel of AECC Shenyang Engine Research Institute. The ice wind tunnel includes a refrigeration system, a water spray atomization system, an aerodynamic system, and a test section. The icing weather conditions of the current ice wind tunnel is: air speed from 0 to 200 m/s, airflow temperature down to -35 ℃, MVD from 15 to 35 μm and LWC from 0.2 to 3.9 g/m³.

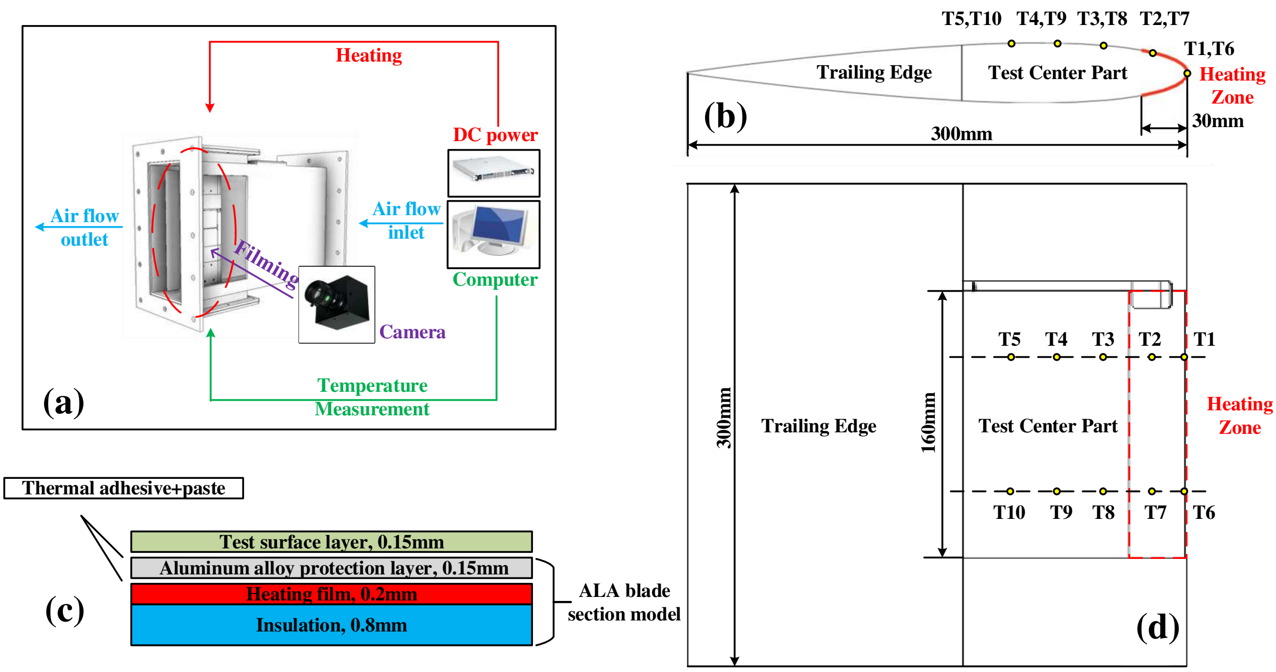

Fig. 3. (**a**) Experimental setup for ice wind tunnel test; (**b**) Sectional view and (**d**) Front view of heating zone and thermocouple arrangement; (**c**) ALA blade section model at heating zone;

The experimental settings can be seen in **Fig. 3**. A digital camera (VP-CCN-100G, Pomeas) was used to capture the ice formation of the testing surface. A power supply (RMX-4122 DC, National Instruments) was used to control the heating power. A data acquisition system (PXIe-4353, National Instruments) was employed to record the temperature change of the thermocouples. The power supply and the data acquisition were connected to the host computer (PXIe-1088, National Instruments). The size of test section was 930mm×230mm×570mm, as shown in **Fig. 3(a)**. The airfoil (NACA 0012) for the icing test in coming experiment had chord length of 300mm and wingspan length of 300mm, as shown in **Fig. 3(b)** and **(d)**. The two ends of the blade model were connected with the fixtures which is installed in the upper and lower walls of the test section, and there were not gaps between the model and the wall of the test section. The area enclosed by the red dotted line in the figure was the anti-icing heating zone, which had projected size of 30mm in the chordwise (10% of the chord length) and 160mm in the spanwise covering the impact zone of water droplets at the leading edge, as shown in **Fig. 3(d)**. The heating zone was arranged symmetrically along the central axis of the airfoil, which was consistent with previous experimental investigation[35]. In order to maintain a high-quality flatness of the testing surface, a groove with depth of 1mm was designed in the anti-icing heating zone, inside which were 0.8 mm polyester film insulation layer and 0.2mm electric heating film. In order to facilitate the replacement of the surface and prevent damage to the heating film, aluminum alloy protective layer with thickness of 0.15 mm was adhered. The test surface layer (four kinds of prepared surfaces in **Table 1**) with thickness of 0.15 mm would be adhered to the outer layer before the experiment, as shown in **Fig. 3(c)**. The thickness of the protective layer and the test surface layer is thin enough that the thermal resistance of ALA in the radial direction is basically the same with that of glass fiber or carbon fiber, which are commonly used in wind turbine blades. Aiming to measure the temperature distribution of the airfoil, 10 type K thermocouples with precision of ±0.1 ℃ (Omega 5TC-TT-K-30-36) were located between the heating film and the aluminum alloy protective layer, as shown in **Fig. 3**(**d**). Among them, the measuring points T1 and T6 were arranged inside the impact zone, T2 and T7 were arranged inside the heating zone but outside the impact zone. The other 6 thermocouples were in the runback zone. The chordwise location of 10 thermocouples are shown in **Table 2**.

Table 2. Chordwise location (x/c) of thermocouples

Thermocouples	**T1,T6**	**T2,T7**	**T3,T8**	**T4,T9**	**T5,T10**
Chordwise Location x/c	0	0.076	0.188	0.277	0.366

2.3 Experimental condition

Four experimental examinations were conducted in the current work. The icing conditions of all the experiments were the same: air speed of 40m/s, LWC of 2g/m^3, air temperature of -7°C, MVD of 20μm, AoA of 0°. The testing surface and heat flux density of the four experiments are shown in **Table 3**. In order to compare the ice protection performance, surface with artificially modified wettability and the base material of ALA were tested in the same experiment.

For instance, in **Test 1** the airfoil was covered by surfaces with material of SP-FNS and ALA, and each of the surfaces took half area of the airfoil, as shown in **Fig. 4** right side. What's more, the heating zone separated the surface into four parts: ALA No Heating, ALA Heating, SP-FNS Heating and SP-FNS No Heating. The heat flux density was 0.7 W/cm^2 for **Test 1** to **Test 3**. In **Test 2** and **Test 3**, the surface prepared by laser ablation method (LA-FS and LA-GT) took larger part of the airfoil area, as shown in **Fig. 5** and **Fig. 6** right side. The surface of ALA with high heat flux density of 3 W/cm^2 was tested in the ice wind tunnel condition, which was named **Test 4**, as shown in **Table 3**.

Table 3. The experimental conditions

No.	Surfaces	Heat flux density (W/cm^2)
Test 1	SP-FNS/ALA	0.7
Test 2	LA-FS/ALA	0.7
Test 3	LA-GT/ALA	0.7
Test 4	ALA	3

3. Results and discussions

3.1 Icing and anti-icing

Fig. 4 shows the icing and anti-icing performance of the electrothermal anti-/de-icing system combined with SP-FNS and ALA (**Test 1**) in the first 120s. As introduced in **Section 2.3**, the upper half part is covered with ALA, the other part is covered with SP-FNS. The ice accumulates immediately on the leading edge without heat source (ALA No heating, SP-FNS No heating), as shown in **Fig. 4** at 15 s. The ice thickness increases with time and the ice shape of the no heating zone shows no difference for ALA and SP-FNS, which indicates that superhydrophobic surface has no contribution to the ice protection when no heat source is applied. This phenomenon is different from the experiments under low airflow velocity[56], which will be carefully discussed in **Section 3.4**. It is observed that at the heat flux density of 0.7 W/cm^2, there is no ice accumulation on the leading edge of the heating zone of ALA, but the runback water freezes seriously on the runback zone, which is typically called wet anti-icing[73]. The heat output maintains the impacted water temperature of the heating zone above the freezing point, resulting in no icing on the heating zone. It is worth noting that the runback water freezes after flowing out of the heating zone for a certain distance. The runback water on ALA forms rivulet, which exchanges heat with the cold surface and the airflow, causing the temperature drops gradually to freezing point and then ice starts to accumulate. This will be further discussed in **Section 3.2**. However, there is no icing on SP-FNS (leading edge or runback zone) when the heat flux density is the same, which is defined as superhydrophobic-dry anti-icing in the current work. For superhydrophobic surface, some researchers[57-60] believed that there are two reasons why it has the capability of anti-icing: **i**) super-cooled water droplets impact the surface and bounce back into the external airflow; **ii**) the impacting droplets form runback water and flow along the airfoil surface to shed from the surface, leaving no ice on the runback zone. We believe that the second explanation should be responsible for the efficient ice protection performance of superhydrophobic surface, which will be further explained in **Section 3.4**.

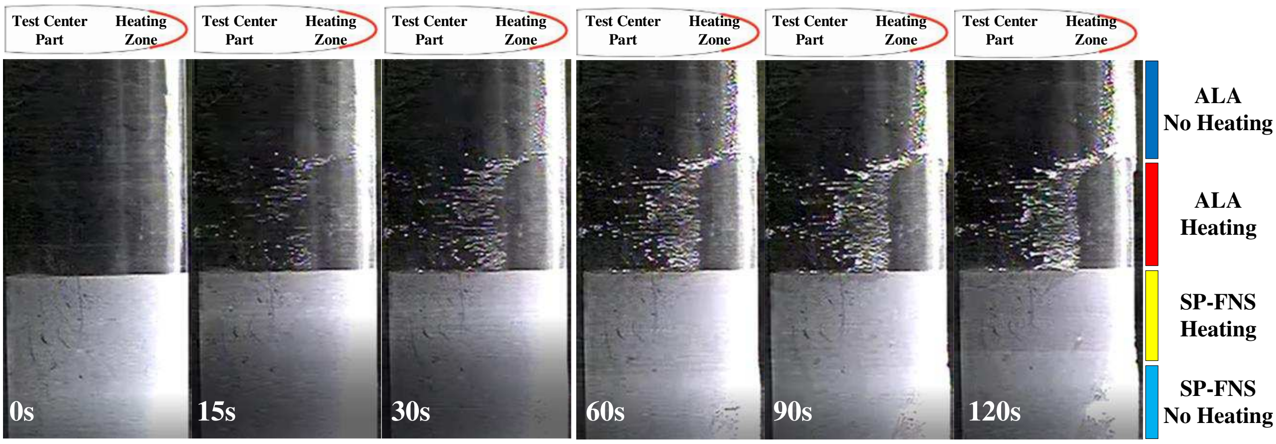

Fig. 4. Image sequence of icing and anti-icing in **Test 1** (0.7 W/cm^2 in heating zone)

In order to compare the ice protection performance between superhydrophobic surfaces from different preparation methods, the LA-FS and ALA surfaces have been tested under the same heating and ice wind tunnel conditions (**Test 2**). The image sequence of icing and anti-icing can be seen in **Fig. 5**. As the icing and anti-icing performance of ALA has been validated in **Test 1**, the spanwise heating area ratio of ALA has been shortened for better investigation of other artificially manufactured surfaces, as introduced in **Section 2.3**. It is observed that at the heat flux density of 0.7W/cm^2, the results are believed to be the same with those of **Test 1**, i.e., there is no icing on LA-FS, and the runback water freezes seriously on ALA. This concludes that the preparation methods may have no influence on the ice protection characteristics of superhydrophobic surfaces, and the surface wettabilities (i.e., contact angle>150° and sliding angle<5°) should be responsible for the efficient anti-icing capability.

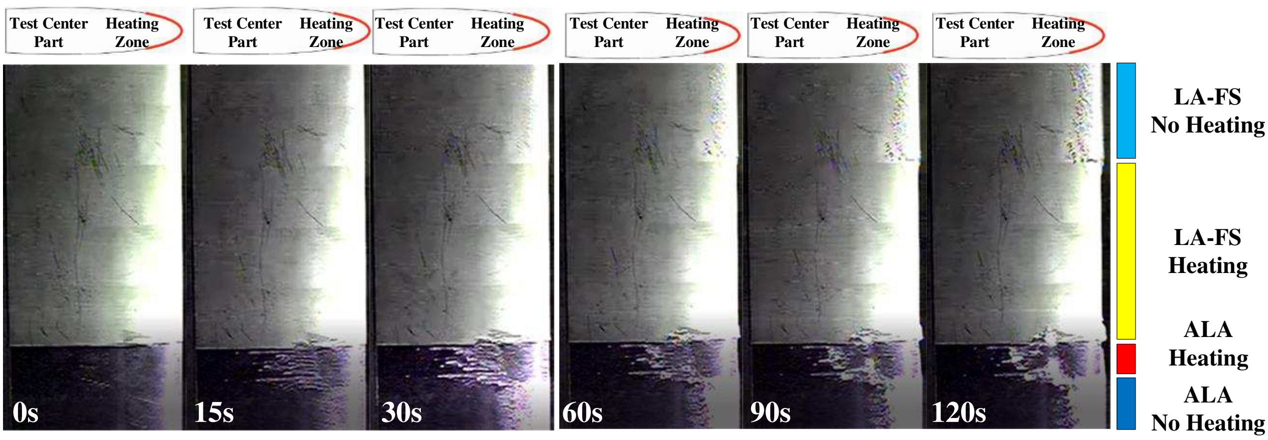

Fig. 5. Image sequence of icing and anti-icing in **Test 2** (0.7 W/cm^2 in heating zone)

It is natural to wonder if only superhydrophobic surface can prevent ice accumulation on airfoil surface. For the current work, the hydrophobic surface (i.e., LA-GT with contact angle of 112.7° and sliding angel of 16.8°) has been tested, the results are shown in **Fig. 6**. There is ice formation on the runback zone for LA-GT, which is almost the same with that of ALA. It's positive to conclude that superhydrophobic surface has the better performance in ice protection than that of hydrophobic surface for the current work, which is consistent with the results presented by previous studies[35, 58, 59, 68, 69]. However, how to answer the question above (i.e., what's the minimum contact angle of hydrophobic surface which can prevent icing) still lacks experimental data, which will be carefully investigated in our future work.

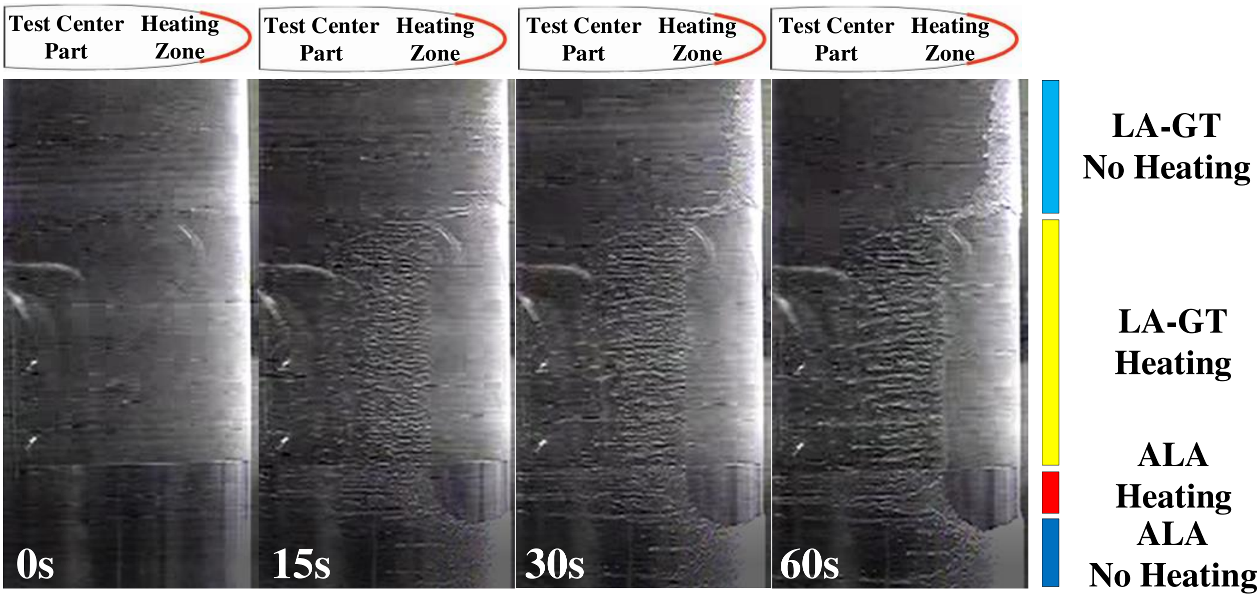

Fig. 6. Image sequence of icing and anti-icing in **Test 2** (0.7 W/cm^2 in heating zone)

Aiming to prevent icing on the airfoil ALA surface completely, the heat flux density is elevated to 3 W/cm^2. The image sequence of icing and anti-icing in **Test 4** is shown in **Fig. 7**. Icing still happens on the runback zone when the temperature of the leading edge is very high (i.e., 68.6℃, as shown in **Table 5**.). What's interesting, the start point of runback ice is delayed when comparing with that of ALA with low heat flux density (e.g., 0.7 W/cm^2 in **Test 1**, as shown in **Fig. 4**). The reason is that the over heated runback water extends the freezing time when flowing downstream, which will be discussed in **Section 3.2**.

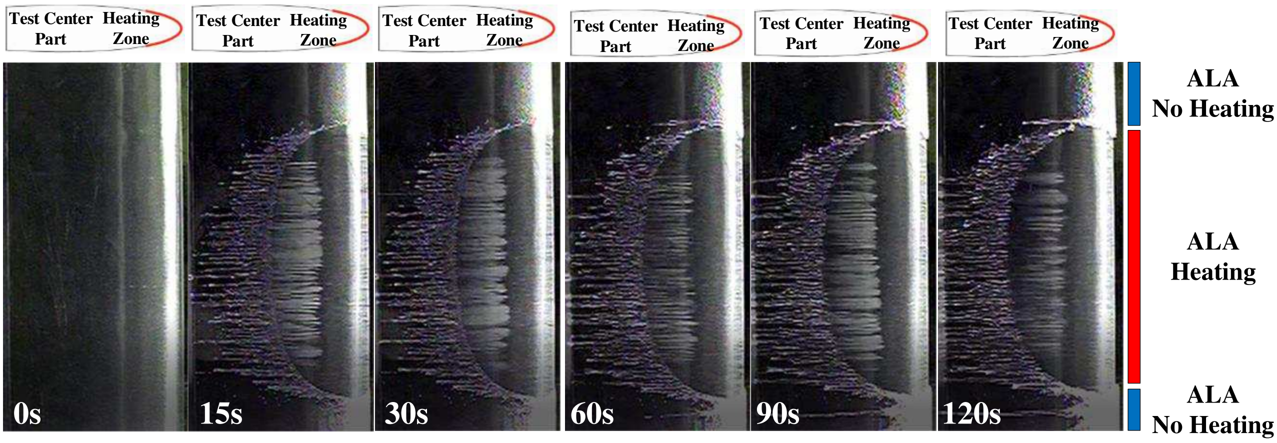

Fig. 7. Image sequence of icing and anti-icing in **Test 4** (3 W/cm^2 in heating zone)

3.2 Temperature distribution and runback icing

Fig. 8 shows the change of temperature profile captured by the thermocouples (as introduced in **Section 2.2**) from **Test 1** to **Test 4**. As shown in **Fig. 8**(**a**), the temperature of the heating zone (T1 and T2 on ALA, T6 and T7 on SP-FNS) is stabilized (around 20°C) in the cold airflow (around -7°C) before the droplets spraying, when the heat flux density (0.7 W/cm^2) is continuously applied. The temperature in the runback zone (T3~T5 on ALA, T8 ~T10 on SP-FNS) maintains around 0 ℃ before the spraying. As shown at ~10 s, the temperature of the heating zone drops immediately when the droplets spraying is on, which is mainly due to the heat sink brought by the supercooled water droplets impacting on the leading edge. As LA-FS or LA-GT covers all the thermocouples (as introduced in **Section 2.2** and **2.3**), the temperature has been averaged for the thermocouples located in the same zone, as shown in **Fig. 8**(**b**) and **Fig. 8**(**c**). When the heat flux density is 3 W/cm^2, the temperature at the heating zone of ALA reaches around 90℃ before the spraying, as shown in **Fig. 8**(**d**). We didn't perform experiment with higher heat flux density than 3 W/cm^2, in order to protect the heating film from high temperature.

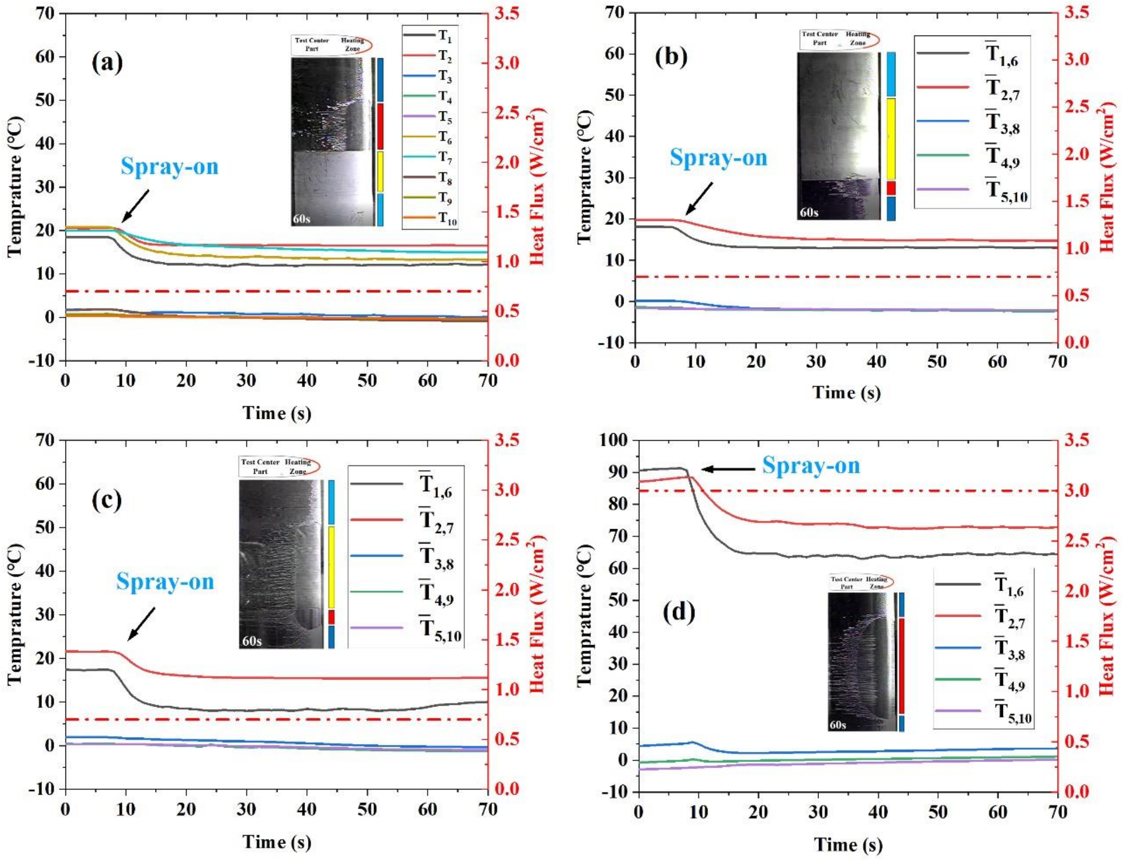

Fig. 8. Temperature profile changing with time during the experiments (**a**) **Test 1** (**b**) **Test 2** (**c**) **Test 3** (**d**) **Test 4**

The runback icing is closely related to the temperature variation along the downstream water flow. The location where icing starts together with the temperature distribution have be analyzed, as shown in **Fig. 9**. **Fig. 9**(**a**) shows the temperature of measured points on different material surfaces at heat flux density of 0.7 W/cm^2. The temperature of measuring points on all of the four surfaces is similar. The average temperature $((\bar{T}_{1,6}+\bar{T}_{2,7})/2)$ of the heating zone on SP-FNS and LA-FS are 14.1℃ and 13.9℃, respectively. The supercooled water droplets impact the leading edge and flow downstream to the runback zone, the temperature increases with heating and reaches a peak value then. So, in the heating zone, the average temperature ($\bar{T}_{2,7}$) at the downstream measuring points is higher than that ($\bar{T}_{1,6}$) of the stagnation points at the leading edge. According to our previous research[74], the temperature of water flow drops quickly when passing the heating zone. The temperature in the runback zone ($\bar{T}_{3,8}$, $\bar{T}_{4,9}$, $\bar{T}_{5,10}$) of all four surfaces is less than zero. However, runback icing has been found only on ALA when heat flux density is 0.7 W/cm^2. What's more, the runback water does not freeze until a certain distance after flowing out of the heating zone, as shown in **Fig. 9**(**a**) (i.e., heating zone ends at 0.1 x/c, runback icing starts at 0.14 x/c), which is typically a wet anti-icing state. According to **Fig. 9**(**b**), the average temperature in the heating zone of ALA is 68.6℃ at heat flux density of

3 W/cm^2, 60 seconds after spraying. Though the temperature of the runback zone is higher than 0°C, runback icing happens eventually (runback icing starts at 0.28 x/c), which should be related to the thermal resistance between the thermocouples and the testing surface.

The runback distance has been doubled in **Test 4** compared with that of ALA at heat flux density of 0.7 W/cm^2. As the heat flux increases, the position where runback icing starts is delayed because the supercooled water droplets are heated to a higher temperature in the heating zone, then reform into the water film which flows towards to the runback zone. After a certain distance, the water film breaks into rivulet flow along the surface of ALA with convective heat transfer to the surface and the cold air, caused by the shear stress from the high speed airflow[26]. The temperature of water gradually drops to the freezing point and then runback ice forms eventually. It's believed that the runback distance of heated water should be further extended if the heat flux input in the heating zone continuously increases. At wet anti-icing state, hazardous runback ice will be reduced when heat input is increased. What's more, the evaporation of water film (or rivulet flow) will be enhanced as the heat flux density increases. When the heat flux density increases to a certain critical value, the supercooled water droplets impact the leading edge and then evaporate into airflow. Certainly, the critical value of heat input is larger than 3 W/cm^2 for the current icing condition in this work, to reach a dry anti-icing state[73] for ALA surface.

As analyzed above, aiming to achieve the dry anti-icing performance, large amount of heat input will cause tremendous energy consumption for traditional material surfaces (i.e., ALA in the current work). Differently, the superhydrophobic-dry anti-icing concept brings a very promising prospect for ice protection system with low energy consumption. The critical point for dry anti-icing is to solve the issue of runback icing. For superhydrophobic-dry anti-icing (i.e., SP-FNS in **Test 1** and LA-FS in **Test 2**), with low energy input (0.7 W/cm^2 in current work), the water leaves the superhydrophobic surface shortly after impacting under the coupled stress of interfacial force and shear stress, preventing the runback icing. The difference between traditional dry anti-icing and superhydrophobic-dry anti-icing relies on the way to disappear the runback liquid water: the former consumes energy to evaporate the water while the latter sheds-off the liquid water spontaneously due to the unique surface wettability.

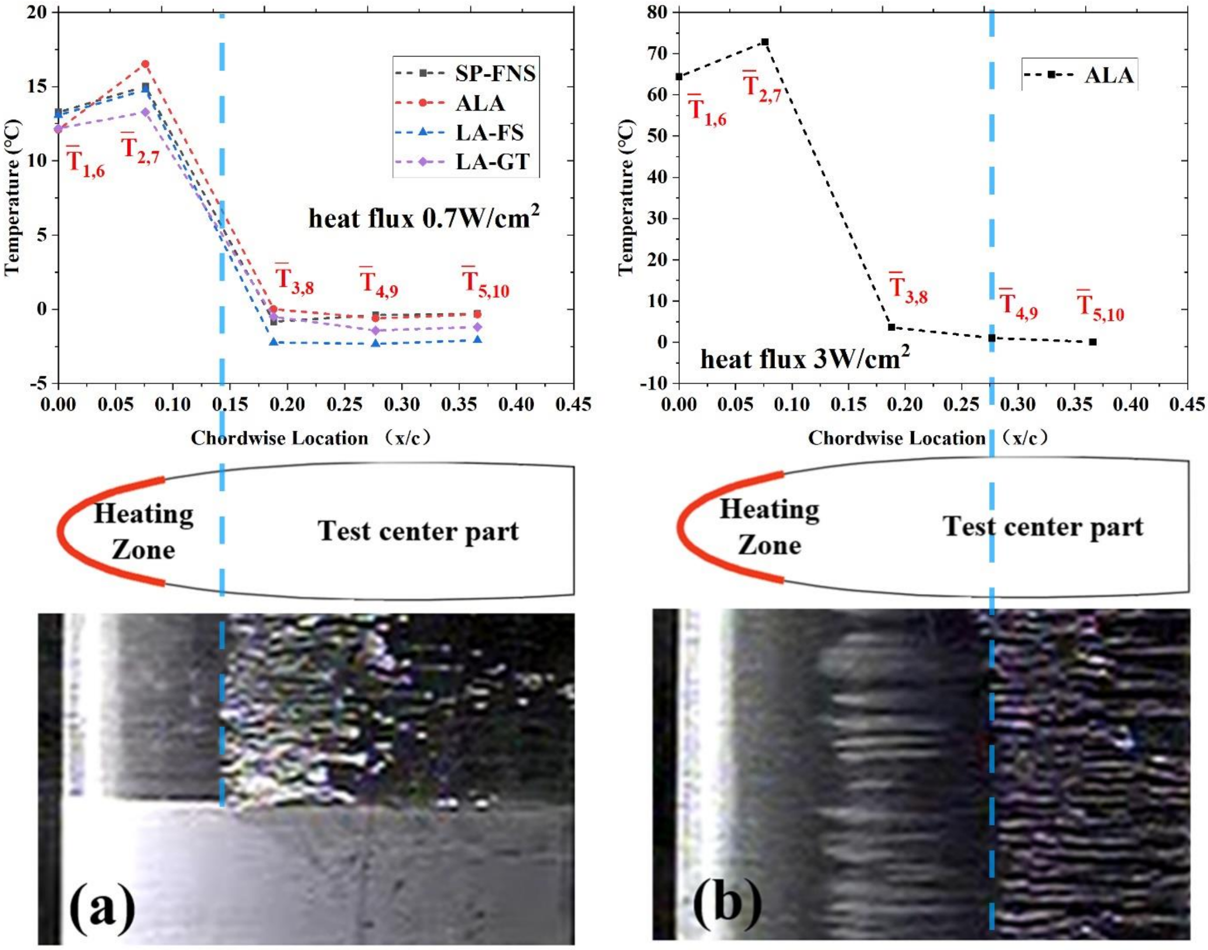

Fig. 9. Temperature variation with x coordinate and runback ice of ALA at (**a**) 0.7 W/cm^2 heat flux density; (**b**) 3 W/cm^2 heat flux density, the capture time is 60 s after spraying.

3.3 Surface wettability induced reduction of energy consumption

As analyzed above, the energy consumption of electrothermal anti-/de-icing system combined with different surfaces is obtained, as shown in **Table 4**. Aiming to achieve the dry anti-icing state (no icing in the heating zone or the runback zone), the critical anti-icing heat flux density should be $\leq$0.7 W/cm^2 for SP-FNS and LA-FS (superhydrophobic surface), larger than 0.7 W/cm^2 for LA-GT (hydrophobic surface) and larger than 3 W/cm^2 for ALA (hydrophilic surface). It can be concluded that the reduction ratio of energy consumption for superhydrophobic-dry anti-icing is larger than 76.7%, which is consistent with the results presented by Hu et al., where the energy consumption of superhydrophobic surface can be reduced by up to 90%[35] in comparison to the hydrophilic surface. In the future work, the precise critical anti-icing heat flux density for superhydrophobic and hydrophobic surface based dry anti-icing should be investigated for different icing conditions, to comprehensively characterize the performance of surface wettability induced ice protection.

Table 4. Critical anti-icing heat flux density of dry anti-icing for different surfaces

Surfaces	SP-FNS	LA-FS	LA-GT	ALA
Critical anti-icing heat flux density of dry anti-icing(W/cm^2)	≤0.7	≤0.7	>0.7	>3
Reduction ratio of energy consumption	>76.7%	>76.7%	/	/

3.4 Ice protection characteristics

There are four experiments conducted in the current work, which includes 14 different testing conditions when surface wettability, preparation method and heat flux density are under consideration. The ice protection characteristics of different conditions are shown in **Table 5**. According to the results listed, passive anti-icing combined with superhydrophobic surface (i.e., superhydrophobic surface without heating) is ineffective, which is consistent with previous works[57, 58]. For active anti-icing, at least 0.7 W/cm^2 heat flux density should be supplied in the heating zone. There should be three active anti-icing states for the experiments: wet anti-icing, dry anti-icing and superhydrophobic-dry anti-icing. When wet anti-icing happens, runback water freezes to ice and may threaten the aerodynamic safety of the airfoil. Dry anti-icing should be the priority choice when considering ice protection for wind turbine blade or aircraft. The traditional dry anti-icing cannot be reached in the present work due to the experimental safety considerations (the heat flux density should be higher than 3 W/cm^2). Fortunately, the superhydrophobic-dry anti-icing has been reached when heated superhydrophobic surfaces are employed (SP-FNS and LA-FS).

The surface wettabilities have significant influence on the ice protection characteristics. Basically, superhydrophobic surface will dramatically reduce the heating power input for dry anti-icing (at least 76.7% in current work). What's more, it seems that hydrophobic surface hasn't shown any benefit for the ice protection system (this conclusion may be changed when heat flux density is increased, which will be carefully investigated in our future work). However, the preparation methods (i.e., spraying method and laser ablation method) of superhydrophobic surfaces may not affect the anti-icing performance.

Table 5. Ice protection characteristics of different experiments

Number	Zone	Heat flux (W/cm^2)	Icing(Y/N)		Anti-icing state	Temperature(℃)	
			Heating zone	Runback zone		Heating zone	Runback zone
Test 1	SP-FNS heating	0.7	N	N	Superhydrophobic-	14.1	-0.5

					dry anti-icing		
	ALA heating	0.7	N	Y	Wet anti-icing	14.3	-0.3
	SP-FNS no heating	0	Y	N	/	/	/
	ALA no heating	0	Y	N	/	/	/
Test 2	LA-FS heating	0.7	N	N	Superhydrophobic-dry anti-icing	13.9	-2.2
	ALA heating	0.7	N	Y	Wet anti-icing	/	/
	LA-FS no heating	0	Y	N	/	/	/
	ALA no heating	0	Y	N	/	/	/
Test 3	LA-GT heating	0.7	N	Y	Wet anti-icing	12.7	-1.0
	ALA heating	0.7	N	Y	Wet anti-icing	/	/
	LA-GT no heating	0	Y	N	/	/	/
	ALA no heating	0	Y	N	/	/	/
Test 4	ALA heating	3	N	Y	Wet anti-icing	68.6	1.6
	ALA no heating	0	Y	N	/	/	/

It's natural to ask why and how the superhydrophobic surface is beneficial for the ice protection system. As mentioned in the introduction section, there are two possible mechanisms[57-60]:

i) supercooled water droplets rebound into the external airflow after impacting the leading edge. This may explain the anti-icing of superhydrophobic surface against the gravity-drived droplet impacting, when the impacting velocity is less than 5 m/s[56]. However, the impacting velocity in the current work is around 40 m/s (Weber number is around 440), deposition or splash of water droplet should happen instead of rebounding. In addition, the temperature drop after the spraying is almost the same for ALA and SP-FNS (as shown in **Fig. 8(a)** at 10 s), indicating the same heat sink brought by supercooled water droplets (i.e., no rebounding from the superhydrophobic surface of SP-FNS). The non-rebounding behavior of supercooled water droplets fails the first mechanism for explaining the current question. What's more, the non-rebounding behavior should also be responsible for the same icing condition of ALA and SP-FNS at the leading edge without heating, let alone that the deposited ice at the leading edge will disable the superhydrophobic wettability immediately after icing happens.

ii) the impacting water droplets reform into liquid water flow and shed from the superhydrophobic surface before runback icing. Normally, the coupled force of surface tension and airflow shear stress will dramatically change the hydrodynamic behavior of liquid water when superhydrophobic surface participates. The droplets impact the heated leading edge and are heated to a relatively high temperature (i.e., 14.1℃ as shown in **Table 5**). The droplets then form the runback water to flow downstream and shed from the surface shortly due to the superhydrophobic wettability, which can be demonstrated that there is no icing on the tailing edge (ALA, hydrophilic) of the airfoil (if the liquid water continuously flow along the surface, runback icing will occur at the tailing edge eventually), as shown in **Fig. 10**. The investigations by Moghtadernejad[75] also shows that under the coupled interfacial force and high-speed shear stress, droplets deform and eventually fly off the superhydrophobic surface instead of flowing along the surface. The quick leaving of liquid water from the superhydrophobic surface prevents the runback icing, which should be responsible for the efficient anti-icing performance with low energy consumption. This is called superhydrophobic-dry anti-icing in the current work.

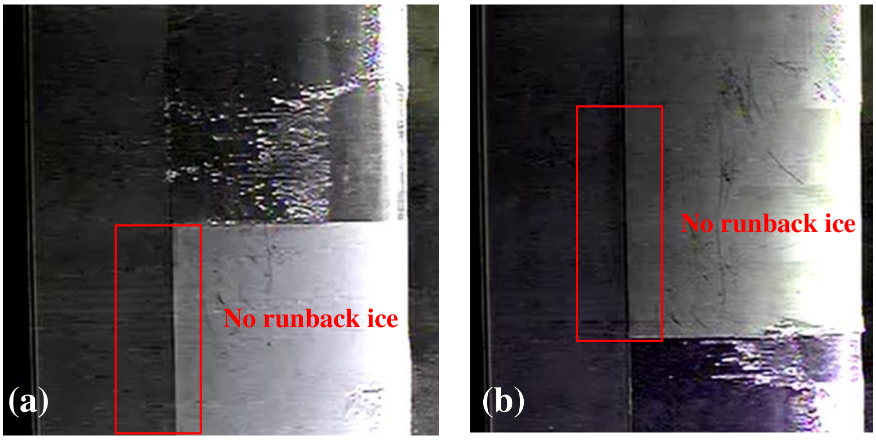

Fig. 10. The image at tailing edge at 60 seconds (**a**) SP-FNS in **Test 1** (**b**) LA-FS in **Test 2**

3.5 Wettability change by droplets impact and water flow

As discussed above, the superhydrophobic surface has outstanding potential in ice protection of wind turbine blade. The durability of the superhydrophobic surfaces should be of great importance to the life cycle application. Test surface layers were removed from the blade model after the test, and then the smooth surface of the leading edge and runback zone were cut into test pieces. The wettability of the surface was tested for five times, and the average value of the five measurements was taken as results, as shown in Fig. 11. The uncertainty level of experimental measurement is judged by the upper and lower limits of repeated measurements. Despite uncertainty level of experimental measurement, the wettability change of the superhydrophobic surface at leading edge and runback zone can still be judged from the measurements. The contact angle and sliding angle of SP-FNS and LA-FS have been compared before and after the ice wind tunnel experiments, the results are shown in **Table 6**.

In comparison to the wettability change of the leading edge and runback zone, it is found that the change of contact angle is relatively small (all above 150°) for both preparation methods. However, a distinct change of the sliding angle has been noticed after the wind ice tunnel experiments (i.e., the sliding angle is all above 5° after the experiment for two zones of both preparation methods). What's more, the sliding angle at the leading edge increases more affectd by droplets impact (i.e., 4.5° to 18.9° for SP-FNS, 3.0° to 9.2° for LA-FS), than that at the runback zone induced by water flow (i.e., 4.5° to 8.0° for SP-FNS, 3.0° to 5.6° for LA-FS). This indicates that the damage of superhydrophobic surfaces from droplets impacting is more serious than that from water flow. In general, the wettability of LA-FS changes less than that of SP-FNS, making the superhydrophobic surface prepared by laser ablation method has better durability.

Table 6. The wettability change of superhydrophobic surfaces

Wettabilities	Before the experiment	After the experiment at leading edge	After the experiment at runback zone
Contact angle of SP-FNS(°)	153.4±2	150.3±2	152.7±2
Sliding angle of SP-FNS(°)	4.5±2	18.9±2	8.0±2
Contact angle of LA-FS(°)	156.0±2	152.4±2	154.1±2
Sliding angle of LA-FS(°)	3.0±2	9.2±2	5.6±2

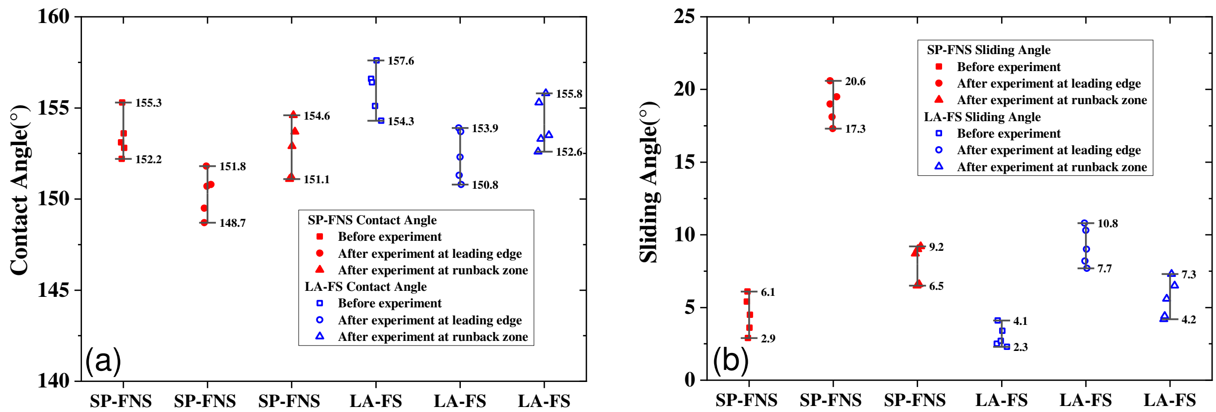

Fig. 11. The measurements of wettabilities (**a**) contact angle (**b**) sliding angle

4. Conclusions

In this paper, the surface wettability induced anti-icing characteristics have been investigated in ice wind tunnel experimentally. Two kinds of superhydrophobic surfaces prepared by spraying method and laser ablation method, one kind of hydrophobic surface prepared by laser ablation method have been fabricated. A test section with electrothermal anti-icing system and temperature acquisition system has been developed for wind ice tunnel experiments. With the consideration of surface wettability, preparation method and heat flux density, the performance of icing and anti-icing under 14 different testing conditions has been validated. The temperature distribution and runback icing have been carefully analyzed, together with the surface wettability induced reduction of energy consumption. Three different anti-icing states (wet anti-icing, dry anti-icing and superhydrophobic-dry anti-icing) have been compared in detail, through the ice protection characteristics from different testing conditions. Furthermore, the mechanism behind the superhydrophobic surface-enhanced ice protection performance has been proposed and validated. The wettability change by droplets impact and water flow has been discussed for analyzing the durability of superhydrophobic surfaces.

Through the investigations above, the conclusions can be reached below:

(1) Passive anti-icing of superhydrophobic surfaces without heating has no effective contribution to ice protection. The energy consumption of electrothermal anti-icing system combined with superhydrophobic surfaces (i.e., active anti-icing) can be dramatically reduced (as much as 76.7%), when the surface temperature is 15℃.

(2) The coupled force of surface tension and airflow shear stress will dramatically change the hydrodynamic behavior of liquid water when superhydrophobic surface participates, which should be responsible for the quick detachment of liquid water from the heating surface, preventing the runback icing.

(3) The anti-icing characteristics can be significantly affected by the surface wettability. Hydrophobic surface shows no advantage for the ice protection. The preparation methods (spraying method and laser ablation method) do not affect the performance of superhydrophobic surfaces. The superhydrophobic-dry anti-icing is believed to have the most potential in developing energy-friendly ice protection system.

(4) Wettability change of the superhydrophobic surfaces shows that the droplets impacting threatens the durability at the leading edge. Compared with the contact angle, the damage on the sliding angle is more serious. The superhydrophobic surface prepared by laser ablation method shows more stable durability than that by spraying method.

Aiming to reduce the energy consumption of ice protection system for wind turbine blade, superhydrophobic-dry anti-icing state should be carefully investigated in the future work. The minimum contact angle of hydrophobic surface which can prevent icing is still unknown, which needs more experimental data. The critical anti-icing heat flux density for superhydrophobic and hydrophobic surface based dry anti-icing should be investigated for different icing conditions, to comprehensively characterize the performance of surface wettability induced ice protection. The detachment of liquid water from the superhydrophobic surface, including hydrodynamic behaviors and coupled heat transfer characteristics, are very interesting for future investigation.

Acknowledgement

This work was supported by the National Natural Science Foundation of China (No. 51906010) and the National Numerical Wind tunnel (Grant 2018-ZT3A05).

References

[1] A. Chehouri, R. Younes, A. Ilinca, J. Perron, Review of performance optimization techniques applied to wind turbines, Applied Energy 142 (2015) 361-388.

[2] J. Lee, F. Zhao, Global Wind Report 2021, Global Wind Energy Council, 2021, p. 80.

[3] L. Battisti, Wind turbines in cold climates: Icing Impacts and Mitigation Systems, Springer International Publishing, 2015.

[4] S.C. Pryor, R.J. Barthelmie, Climate change impacts on wind energy: A review, Renewable and Sustainable Energy Reviews 14(1) (2010) 430-437.

[5] Q. Wang, X. Yi, Y. Liu, J. Ren, W. Li, Q. Wang, Q. Lai, Simulation and analysis of wind turbine ice accretion under yaw condition via an Improved Multi-Shot Icing Computational Model, Renewable Energy 162 (2020) 1854-1873.

[6] Q. Wang, J. Xiao, T. Zhang, J. Yang, Y. Shi, A new wind turbine icing computational model based on Free Wake Lifting Line Model and Finite Area Method, Renewable Energy 146 (2020) 342-358.

[7] E. Madi, K. Pope, W. Huang, T. Iqbal, A review of integrating ice detection and mitigation for wind turbine blades, Renewable and Sustainable Energy Reviews 103 (2019) 269-281.

[8] G. Fortin, J. Perron, Wind Turbine Icing and De-Icing, 47th AIAA Aerospace Sciences Meeting including The New Horizons Forum and Aerospace Exposition, 2009.

[9] M.G. Potapczu, A review of NASA Lewis' development plans for computational simulation of aircraft icing, 37th Aerospace Sciences Meeting and Exhibit, Reno, NV, 1999, p. 15.

[10] M.C. Homola, M.S. Virk, P.J. Nicklasson, P.A. Sundsbø, Performance losses due to ice accretion for a 5 MW wind turbine, Wind Energy 15(3) (2012) 379-389.

[11] M.S. Virk, M.C. Homola, P.J. Nicklasson, Atmospheric icing on large wind turbine blades, International Jurnal of Energy & Environment 3(1) (2012) 1-8.

[12] T. Reid, G. Baruzzi, I. Ozcer, D. Switchenko, W. Habashi, FENSAP-ICE Simulation of Icing on Wind Turbine Blades, Part 1: Performance Degradation, 51st AIAA Aerospace Sciences Meeting including the New Horizons Forum and Aerospace Exposition, 2013.

[13] F. Lamraoui, G. Fortin, R. Benoit, J. Perron, C. Masson, Atmospheric icing impact on wind turbine production, Cold Regions Science and Technology 100 (2014) 36-49.

[14] L. Shu, G. Qiu, Q. Hu, X. Jiang, G. McClure, Y. Liu, Numerical and experimental investigation of threshold de-icing heat flux of wind turbine, Journal of Wind Engineering and Industrial Aerodynamics 174 (2018) 296-302.

[15] J.Y. Jin, M.S. Virk, Study of ice accretion and icing effects on aerodynamic characteristics of DU96 wind turbine blade profile, Cold Regions Science and Technology 160 (2019) 119-127.

[16] O. Yirtici, K. Cengiz, S. Ozgen, I.H. Tuncer, Aerodynamic validation studies on the performance analysis of iced wind turbine blades, Computers & Fluids 192 (2019).

[17] C. Son, M. Kelly, T. Kim, Boundary-layer transition model for icing simulations of rotating wind turbine blades, Renewable Energy 167 (2021) 172-183.

[18] R. Manatbayev, Z. Baizhuma, S. Bolegenova, A. Georgiev, Numerical simulations on static Vertical Axis Wind Turbine blade icing, Renewable Energy 170 (2021) 997-1007.

[19] L. Hu, X. Zhu, C. Hu, J. Chen, Z. Du, Wind turbines ice distribution and load response under icing conditions,

Renewable Energy 113 (2017) 608-619.

[20] B.L. Messinger, Equilibrium Temperature of an Unheated Icing Surface as a Function of Air Speed, Journal of the Aeronautical Sciences 20(1) (1953) 29-42.

[21] T.G. Myers, C.P. Thompson, Modeling the Flow of Water on Aircraft in Icing Conditions, AIAA Journal 36(6) (1998) 1010-1013.

[22] T.G. Myers, Extension to the Messinger Model for Aircraft Icing, AIAA Journal 39(2) (2001) 211-218.

[23] Y. Bourgault, W. Habashi, H. Beaugendre, Development of a shallow water icing model in FENSAP-ICE, 37th Aerospace Sciences Meeting and Exhibit, Reno, NV, 1999, p. 10.

[24] A.G. Kraj, E.L. Bibeau, Phases of icing on wind turbine blades characterized by ice accumulation, Renewable Energy 35(5) (2010) 966-972.

[25] Y. Li, K. Tagawa, F. Feng, Q. Li, Q. He, A wind tunnel experimental study of icing on wind turbine blade airfoil, Energy Conversion and Management 85 (2014) 591-595.

[26] L. Gao, Y. Liu, W. Zhou, H. Hu, An experimental study on the aerodynamic performance degradation of a wind turbine blade model induced by ice accretion process, Renewable Energy 133 (2019) 663-675.

[27] P. Roberge, J. Lemay, J. Ruel, A. Bégin-Drolet, Field analysis, modeling and characterization of wind turbine hot air ice protection systems, Cold Regions Science and Technology 163 (2019) 19-26.

[28] J.Y. Jin, M.S. Virk, Experimental study of ice accretion on S826 & S832 wind turbine blade profiles, Cold Regions Science and Technology 169 (2020).

[29] T. Reid, G. Baruzzi, I. Ozcer, D. Switchenko, W. Habashi, FENSAP-ICE Simulation of Icing on Wind Turbine Blades, Part 2: Ice Protection System Design, 51st AIAA Aerospace Sciences Meeting including the New Horizons Forum and Aerospace Exposition, 2013.

[30] O. Fakorede, Z. Feger, H. Ibrahim, A. Ilinca, J. Perron, C. Masson, Ice protection systems for wind turbines in cold climate: characteristics, comparisons and analysis, Renewable and Sustainable Energy Reviews 65 (2016) 662-675.

[31] J. Hu, B. Lan, K. Xu, X. Jiang, B. Shi, H. Yang, Wind Tunnel Experimental Study for Anti-icing Performance of Wind Blades with Hydrophobic Coatings, Gaodianya Jishu/High Voltage Engineering 44(3) (2018) 719-726.

[32] A. Azimi Yancheshme, A. Allahdini, K. Maghsoudi, R. Jafari, G. Momen, Potential anti-icing applications of encapsulated phase change material–embedded coatings; a review, Journal of Energy Storage 31 (2020).

[33] B. Wu, X. Cui, H. Jiang, N. Wu, C. Peng, Z. Hu, X. Liang, Y. Yan, J. Huang, D. Li, A superhydrophobic coating harvesting mechanical robustness, passive anti-icing and active de-icing performances, J Colloid Interface Sci 590 (2021) 301-310.

[34] H. Guo, M. Liu, C. Xie, Y. Zhu, X. Sui, C. Wen, Q. Li, W. Zhao, J. Yang, L. Zhang, A sunlight-responsive and robust anti-icing/deicing coating based on the amphiphilic materials, Chemical Engineering Journal 402 (2020).

[35] L. Gao, Y. Liu, L. Ma, H. Hu, A hybrid strategy combining minimized leading-edge electric-heating and superhydro-/ice-phobic surface coating for wind turbine icing mitigation, Renewable Energy 140 (2019) 943-956.

[36] C. Mayer, A. Ilinca , G. Fortin, J. Perron, Icing Wind Tunnel Study of a Wind Turbine Blade Deicing System, International Journal of Offshore & Polar Engineering (2007) 182-188.

[37] J. Sabatier, P. Lanusse, B. Feytout, S. Gracia, CRONE control based anti-icing/deicing system for wind turbine blades, Control Engineering Practice 56 (2016) 200-209.

[38] Y. Ibrahim, R. Kempers, A. Amirfazli, 3D printed electro-thermal anti- or de-icing system for composite panels, Cold Regions Science and Technology 166 (2019).

[39] S. Jung, L.P. Raj, A. Rahimi, H. Jeong, R.S. Myong, Performance evaluation of electrothermal anti-icing systems for a rotorcraft engine air intake using a meta model, Aerospace Science and Technology 106 (2020).

[40] L.B. Boinovich, A.M. Emelyanenko, Anti-icing Potential of Superhydrophobic Coatings, Mendeleev Communications 23(1) (2013) 3-10.

[41] Z. Zhao, H. Chen, X. Liu, H. Liu, D. Zhang, Development of high-efficient synthetic electric heating coating for anti-icing/de-icing, Surface and Coatings Technology 349 (2018) 340-346.

[42] X. Liu, H. Chen, Z. Zhao, Y. Yan, D. Zhang, Slippery liquid-infused porous electric heating coating for anti-icing and de-icing applications, Surface and Coatings Technology 374 (2019) 889-896.

[43] P. Wang, T. Yao, Z. Li, W. Wei, Q. Xie, W. Duan, H. Han, A superhydrophobic/electrothermal synergistically anti-icing strategy based on graphene composite, Composites Science and Technology 198 (2020).

[44] T. Onda, S. Shibuichi, N. Satoh, K. Tsujii, Super-Water-Repellent Fractal Surfaces, Langmuir 12(9) (1996) 2125-2127.

[45] M. Ma, R.M. Hill, Superhydrophobic surfaces, Current Opinion in Colloid & Interface Science 11(4) (2006) 193-202.

[46] P. Roach, N. J. Shirtcliffe, M.I. Newton, Progess in superhydrophobic surface development, Soft Matter 4(2) (2008) 224-240.

[47] C. Peng, S. Xing, Z. Yuan, J. Xiao, C. Wang, J. Zeng, Preparation and anti-icing of superhydrophobic PVDF coating on a wind turbine blade, Applied Surface Science 259 (2012) 764-768.

[48] S.S. Latthe, R.S. Sutar, A.K. Bhosale, S. Nagappan, C.-S. Ha, K.K. Sadasivuni, S. Liu, R. Xing, Recent developments in air-trapped superhydrophobic and liquid-infused slippery surfaces for anti-icing application, Progress in Organic Coatings 137 (2019).

[49] L. Liu, W. Tang, Q. Ruan, Z. Wu, C. Yang, S. Cui, Z. Ma, R.K.Y. Fu, X. Tian, R. Wang, Z. Wu, P.K. Chu, Robust and durable surperhydrophobic F-DLC coating for anti-icing in aircrafts engineering, Surface and Coatings Technology 404 (2020).

[50] L. Lv, H. Liu, W. Zhang, J. Chen, Z. Liu, Facile UV-curable fabrication of robust, anti-icing superhydrophobic coatings based on polyurethane, Materials Letters 258 (2020).

[51] C. Qin, A.T. Mulroney, M.C. Gupta, Anti-icing epoxy resin surface modified by spray coating of PTFE Teflon particles for wind turbine blades, Materials Today Communications 22 (2020).

[52] M. Nosonovsky, B. Bhushan, Superhydrophobic surfaces and emerging applications: Non-adhesion, energy, green engineering, Current Opinion in Colloid & Interface Science 14(4) (2009) 270-280.

[53] T. Maitra, C. Antonini, M. K. Tiwari, A. Mularczyk, Z. Imeri, P. Schoch, D. Poulikakos, Supercooled water drops impacting superhydrophobic textures, Langmuir 30(36) (2014) 10855-61.

[54] D. Richard, C. Clanet, D. Quéré, Contact time of a bouncing drop, Nature 417 (2002) 811.

[55] J.C. Bird, R. Dhiman, H.M. Kwon, K.K. Varanasi, Reducing the contact time of a bouncing drop, Nature 503(7476) (2013) 385-388.

[56] C. Antonini, F. Villa , I. Bernagozzi, A. Amirfazli, M. Marengo, Drop rebound after impact: the role of the receding contact angle, Langmuir 29(52) (2013) 16045-50.

[57] S. Kimura, Y. Yamagishi, A. Sakabe, T. Adachi, M. Shimanuki, A New Surface Coating for Prevention of Icing on Airfoils, 2007 SAE Aircraft & Engine Icing International Conference, Seville, Spain, 2007, p. 7.

[58] G. Fortin, M. Adomou, J. Perron, Experimental Study of Hybrid Anti-Icing Systems Combining Thermoelectric and Hydrophobic Coatings, SAE Technical Paper Series (2011) 281-283.

[59] C. Antonini, M. Innocenti, T. Horn, M. Marengo, A. Amirfazli, Understanding the effect of superhydrophobic coatings on energy reduction in anti-icing systems, Cold Regions Science and Technology 67(1-2) (2011) 58-67.

[60] K. Knausgård, Superhydrophobic Anti-Ice Nanocoatings, Department of Structural Engineering, Norwegian University of Science and Technology 2012, p. 146.

[61] M. Liravi, H. Pakzad, A. Moosavi, A. Nouri-Borujerdi, A comprehensive review on recent advances in superhydrophobic surfaces and their applications for drag reduction, Progress in Organic Coatings 140 (2020).

[62] A. A. Yancheshme, G. Momen, R. Jafari Aminabadi, Mechanisms of ice formation and propagation on superhydrophobic surfaces: A review, Advances in Colloid and Interface Science 279 (2020).

[63] L. Ge, G. Ding, H. Wang, J. Yao, P. Cheng, Y. Wang, Anti-Icing Property of Superhydrophobic Octadecyltrichlorosilane Film and Its Ice Adhesion Strength, Journal of Nanomaterials 2013 (2013) 1-5.

[64] S. Yang, Q. Xia, L. Zhu, J. Xue, Q. Wang, Q. Chen, Research on the icephobic properties of fluoropolymer-

based materials, Applied Surface Science 257(11) (2011) 4956-4962.

[65] S. Lei, X. Fang, J. Ou, F. Wang, M. Xue, W. Li, A. Amirfazli, S.F. Chini, Icing of static and high-speed water droplets on superhydrophobic surface, Materials Letters 285 (2021).

[66] M. Susoff, K. Siegmann, C. Pfaffenroth, M. Hirayama, Evaluation of icephobic coatings—Screening of different coatings and influence of roughness, Applied Surface Science 282 (2013) 870-879.

[67] Y. H. Yeong, J. Sokhey, E. Loth, Ice Adhesion on Superhydrophobic Coatings in an Icing Wind Tunnel, Contamination Mitigating Polymeric Coatings for Extreme Environments (2018) 99-121.

[68] D. De Pauw, A. Dolatabadi, Effect of Superhydrophobic Coating on the Anti-Icing and Deicing of an Airfoil, Journal of Aircraft 54(2) (2017) 490-499.

[69] D. Mangini, C. Antonini, M. Marengo, A. Amirfazli, Runback ice formation mechanism on hydrophilic and superhydrophobic surfaces, Cold Regions Science and Technology 109 (2015) 53-60.

[70] C. Cai, N. Sang, S. Teng, Z. Shen, J. Guo, X. Zhao, Z. Guo, Superhydrophobic surface fabricated by spraying hydrophobic R974 nanoparticles and the drag reduction in water, Surface and Coatings Technology 307 (2016) 366-373.

[71] R.M. Waldman, H. Li, H. Hu, An Experimental Investigation on the Effects of Surface Wettability on Water Runback and Ice Accretion over an Airfoil Surface, 8th AIAA Atmospheric and Space Environments Conference, 2016.

[72] J.T. Korhonen, T. Huhtamaki, O. Ikkala, R.H. Ras, Reliable measurement of the receding contact angle, Langmuir 29(12) (2013) 3858-63.

[73] S.J.M. Cabler, Advisory circular no. 20-73A, Aircraft Ice Protection, FAA, 2006, p. 233.

[74] X. Bu, G. Lin, x. Shen, Z. Hu, D. Wen, Numerical simulation of aircraft thermal anti-icing system based on a tight-coupling method, International Journal of Heat and Mass Transfer 148 (2020).

[75] S. Moghtadernejad, M. Mohammadi, M. Jadidi, M. Tembely, A. Dolatabadi, Shear Driven Droplet Shedding on Surfaces with Various Wettabilities, SAE International Journal of Aerospace 6(2) (2013) 459-464.